Journal of Applied Sciences

ISSN 1812-5654

science alert

ANSInet
an open access publisher
http://ansinet.com

OPEN ACCESS Journal of Applied Sciences

ISSN 1812-5654
DOI: 10.3923/jas.2022.217.232

Research Article
A New Coefficient of Discharge Relation for Flow Over Broad-Crested Rectangular Side Weir in a Trapezoidal-Type Channel

[1]Amirhosein Sarchami, [1]Mahdi Tousi, [2]Hossein Afshar and [3]Goodarz Ahmadi

[1]Department of Mechanics, Electrical Power and Computer, Science and Research Branch, Islamic Azad University, Tehran, Iran
[2]Department of Mechanical Engineering, East Tehran Branch, Islamic Azad University, Tehran, Iran
[3]Department of Mechanical and Aerospace Engineering, Clarkson University, Potsdam, New York, United States of America

Abstract

Background and Objective: One of the new methods to receive and distribute flow in floodwater spreading systems is utilizing side weirs. These weirs are employed extensively in environmental, irrigation and hydraulics engineering to control the flow direction. This work evaluates the hydraulic behaviour of the rectangular broad-crested side weir in a trapezoidal shape channel numerically and experimentally to calculate the coefficient of discharge. **Materials and Methods:** In this investigation, gene expression programming is employed to predict the discharge coefficient under various conditions. **Results:** The study results revealed that six key factors affect the side weir discharge coefficient, which is the froude number (F_r), main channel's bed slope, side weir step's height to side weir's length $\left(\frac{H}{L}\right)$, the side weir's angle (θ), side weir step's height to upstream flow depth of side weir $\left(\frac{H}{y_1}\right)$ and upstream flow depth of side weir to side weir's length $\left(\frac{y_1}{L}\right)$. The results of nearly 300 experimental tests were compiled to develop a new correlation for predicting the coefficient of discharge under subcritical conditions for a broad-crested side weir. Regression models were used to investigate the connection between the coefficient of discharge and the relevant parameters. The results revealed that the coefficient of discharge was decreased by increasing the and the side weir step's height to the length of the side weir ratio. **Conclusion:** In addition, the coefficient of discharge was increased by increasing the ratio of the side weir flow depth upstream to the height of the side weir step and the ratio of the side weir upstream flow depth to the length of the side weir.

Key words: Coefficient of discharge, trapezoidal open-channel flow, broad-crested rectangular side weir, gene expression programming, measurement, numerical simulation, hydraulics

Citation: Sarchami, A., M. Tousi, H. Afshar and G. Ahmadi, 2022. A new coefficient of discharge relation for flow over broad-crested rectangular side weir in a trapezoidal-type channel. J. Appl. Sci., 22: 217-232.

Corresponding Author: Hossein Afshar, Department of Mechanical Engineering, East Tehran Branch, Islamic Azad University, Tehran, Iran

Competing Interest: The authors have declared that no competing interest exists.

Data Availability: All relevant data are within the paper and its supporting information files.

INTRODUCTION

In general, side weirs are structures employed to divert the fluid flow and are located at the side of an open channel that steers the flow stream to the side channel's direction. Side weirs are primarily deployed for irrigation, land drainage and hydraulic engineering to adjust heads in distributaries and escapes. They are generally designed to operate as a control structure in the open channels and divert a certain amount of discharge. Hence, in the area of measurement of water flows, an approximate evaluation of discharge over the side weirs is still a problem of importance and a novel issue. They are easy to use, precise and traditional devices employed in the laboratory and for measuring flow in open channels[1]. The hydropower aspect and the coefficient of discharge of these side weirs for the various kinds of main channels, flow conditions and weirs have been investigated extensively.

Side weirs come in different types for different applications. Depending on their specific type and usage, side weirs can have various shapes (i.e., triangular, rectangular, trapezoidal, etc.). Additionally, the crest of side weirs can be made broad or sharp. Taking an experimental approach Abbasi *et al*.[2] investigated the effect of geometric variables of the antivortex on a triangular side weir. In addition, the coefficient of discharge of side weir as related to the angle at the climax of the triangular weir and Froude number was described in their effort. The hydraulic performance of sharp-crested rectangular side weirs has been broadly studied in the literature for various scenarios combining different flow conditions and a variety of main channels. Previously[3-7] evaluated the flow behaviour over sharp-crested rectangular side weirs in rectangular main channels. They concluded that the experimental data for subcritical flow agrees well with the derived analytical discharge coefficient. Also, they developed a relationship for the rectangular sharp-crested side weir's coefficient of discharge. In addition, Granata and Marinis[8] studied a dynamic relationship for flow in a rectangular channel along a side weir. They used De Marchi's equation extensively for calculating the rectangular side weir's coefficient of discharge.

Maranzoni *et al*.[9] studied the lateral outflow over rectangular side weir placed in a straight channel based on the specific energy principle. The flow behaviour of a developed oblique side weir in subcritical flow was studied by Borghei and Parvaneh[10] using the principle of specific energy. Their experimental results indicated that the developed oblique side weir is more efficient in comparison to other conventional side weirs. Azimi *et al*.[11] investigated the discharge coefficient of rectangular-shaped side weir placed in a circular channel. To evaluate the coefficient of discharge, they studied the ratio of the side weir's height to the weir's upstream flow depth and the Froude number of upstream. Finally, Afshar and Hosein[12] experimentally investigated a broad-crested rounded corner/rectangular shape side weir. In their investigation, a CFD simulation alongside the laboratory model was performed to determine the free surface profile in broad-crested rectangular shape side weir.

It is clear that nearly all researchers have investigated the fluid flow specifications of triangular/rectangular side weirs; however, little attention has been given to specifications of the hydraulic behavior of trapezoidal shape side weirs. In practical terms, trapezoidal shape channels along a side weir can be employed to manage drainage water and to deliver water to farm fields. Azimi *et al*.[13] investigated the discharge coefficient of the rectangular side weir placed in a trapezoidal channel using support vector machines. They proposed an optimal model based on effective parameters on the discharge coefficient. Nezami *et al*.[14] studied the trapezoidal lateral opening in a rectangular main channel intended for subcritical flow and discovered that the coefficient of discharge is related to the Froude number (F_{r1}). This correlation was also confirmed with experimental tests. Using the principles of specific energy. Vatankhah[15] developed an analytical method to calculate the free surface flow profile along a side weir installed in a trapezoidal shape channel.

Previous studies performed on the typical side weirs suggest that three primary factors influencing their discharge coefficient (C_m). These parameters are the froude number (F_{r1}), the ratios of weir's height to upstream depth and weir's length to channel's width. Earlier, it was assumed that the Froude number was the main parameter affecting the value of C_m. Namaee *et al*.[16] experimentally investigated the fluid flow behaviour of a broad-crested side weir in a rough bed trapezoidal channel under the subcritical flow condition. Their results demonstrated that four primary factors affect the side weir coefficient of discharge and a new equation was proposed. Their equation included the parameters noted above and also the influence of the main channel's bed slope.

The advances in computational fluid dynamics have made numerical simulation a suitable method for studying the free surface flow of devices used for water measurement in free surface channels[17]. Bilhan *et al*.[18] and Emiroglu *et al*.[19,20] investigated the hydraulic characteristics of rectangular, triangular and different trapezoidal shape labyrinth side weirs in subcritical flows. Their results showed that the labyrinth side weir has a noticeably higher coefficient of discharge compared to standard side weirs. A relationship for the calculation of the coefficient of discharge in labyrinth side

weirs was also provided. Aydin and Emiroglu[21] studied the hydrodynamic performance of a two-cycle side weir numerically. They showed that an increase in the upstream Froude number caused a decline in the discharge coefficient. Wang *et al.*[22] studied the hydraulic parameters of side weirs of trapezoidal sharp-crested shape, including the froude number, velocity distribution, water profiles and discharge coefficient. Their results indicated that the simulated water depths were similar to the observation, with a lower than 5.63% relative error.

In the last few years, artificial intelligence (AI) techniques have been applied to predict the behaviour of non-linear systems in different scientific fields. In addition, many scientists have employed soft computing to recognize patterns of various hydraulic phenomena. Taking an experimental approach, Gopakumar and Mujumdar[23] studied the discharge coefficient of rectangular sharp-crested side weirs in a straight channel. A neural network model was developed to calculate the discharge coefficient and the results showed that these techniques could be effectively used in predicting the coefficient of discharge. Ebtehaj *et al.*[24] derived a model for the discharge coefficient of side weirs placed in rectangular shape channels employing the gene expression programming (GEP) model. The value of the correlation coefficient in their presented model was 0.947. Optimization was carried out by Khoshbin *et al.*[25] by employing the singular value analysis and the genetic algorithm (GA) for a neuro-fuzzy inference system for estimating the discharge coefficient of side weirs. Jahanpanah *et al.*[26] predicted the coefficient of discharge of channels with rectangular shapes by applying four soft computing models. The parameters used included the roughness coefficient, the depth of the brink, the channel's bed slope and the channel's width. Experimental data were compared with the computed discharge coefficients for the accuracy test. The results also indicated that the artificial neural network model is more efficient than the other soft computing methods. Azimi *et al.*[27] analyzed the sensitivity of variables that affect the coefficient of discharge of weirs installed in channels with trapezoidal shape by employing the extreme learning machines (ELM) method. It was also shown that the efficacy of the Froude number in estimating the coefficient of discharge is more than other variables. The side weirs installed on channels with trapezoidal shape and their conducting capacity were investigated by Azimi *et al.*[28] using the GEP. It was indicated in their effort that the AI model of 81% of results had an error of less than 5%.

In summary, sharp-crested side weirs are instruments employed to determine the discharge of the water from the small rivers and channels, while in the case of the broad-crested side weirs, large discharge coefficients are measured. Compared with the other main channel shapes, the trapezoidal main channel is quite common due to the advantages such as the capability of large discharge of water, performing very effectively, suitable structure and ease of arrangement. However, so far, the numerical simulations on broad-crested rectangular side weir in trapezoidal channels for studying their hydraulic performance are scarce.

In this study, the flow behaviour of rectangular broad-crested shape side weir in the trapezoidal channel was investigated. The experimental data were used to develop an equation for predicting the discharge coefficient of rectangular broad-crested side weir. Also, computational hydraulic models and gene expression programming were developed to simulate the hydraulic behaviour of rectangular broad-crested side weir under various hydraulic conditions. The developed three-dimensional numerical model effectively captured the principal hydraulic features of broad-crested side weirs. In addition, applying the gene expression programming (GEP) method, the range of the geometrical parameters was extended and the effects of additional discharge coefficients were evaluated. To consider the effect of geometrical parameters (step height, side weir length and side weir angle) on the discharge coefficient, six gene expression programming models were created and their influences on the coefficient of discharge estimation were evaluated. Eventually, the optimal model is achieved and an equation of this model is calculated for use in real applications.

MATERIALS AND METHODS

Basic theory: In Granata and de Marinis[8] investigation, De Marchi's equations theoretically demonstrated that, while the flow profile is curved, the energy head alongside the crest's spillway stays the same, increasing in subcritical flow and decreasing in supercritical flow. An example of a varied flow with decreased discharge in space is the flow over a side weir. The energy equation is generally used for deriving the governing equations of flow over a side weir. French and French[29] derived the main differential equations of a varied flow in space alongside a side weir with a reduction in discharge as:

$$\frac{dy}{dx}=\frac{S_0-S_f-\frac{\alpha Q}{gA^2}\times\frac{dQ}{dx}}{1-\frac{\alpha Q^2T}{gA^3}} \quad (1)$$

In this equation, the is the distance along weir from the end of upstream, represents the flow depth, S_0 is main channel's bed slope, S_f is the slope of friction, is the correction factor of kinetic energy, the discharge of the channel is represented by Q, dQ/dx is the variation of discharge along the side weir length, g is the gravitational acceleration, A is the flows cross-sectional area and T is the channel section top width.

In trapezoidal channels, the cross-section of flow is evaluated using:

$$\frac{dA}{dx} = T\frac{dy}{dx} \quad (2)$$

Also, for a rectangular shape broad-crested side weir assuming that S_0-S_f = 0 and α = 1 the discharge Q per unit length of a rectangular side weir of heights, Eq. 1 is simplified as[29,30]:

$$-\frac{dQ}{dx} = \frac{2}{3}C_m\sqrt{2g}\ (y-S)^{\frac{3}{2}} \quad (3)$$

In which, x is weir's distance from upstream (horizontal distance), y is the height of the side weir, is the depth of flow at the main channel, (y-s) is the pressure head on the weir and C_m is the coefficient of discharge.

In general, introducing the dimensional groups, C_m can be expressed as:

$$C_m = f\left(F_{r1}, S_0, \frac{p}{y_1}, \frac{y_1}{B}\right) \quad (4)$$

In this equation, S_0 is main channel's bed slope, p is the weir height, B is the main channel width, y_1 is the upstream flow depth at the section of the side weir, F_{r1} is the upstream froude number. The functional form of Eq. 4 was evaluated in the experimental phase of the study.

Additional new dimensional parameters are used to assess the influence of all variables affecting the discharge coefficient of side weir in the numerical (CFD/GEP) study of the proposed side weir of broad-crested rectangular shape. These are side weir step's height to side weir's length $\left(\frac{H}{L}\right)$ ratio, side weir angle (θ), ratio of side weir's flow depth upstream to the height of side weir step $\left(\frac{H}{y_1}\right)$ and the ratio of the side weir's flow depth upstream to side weir length $\left(\frac{y_1}{L}\right)$ are considered. Therefore, the dimensionless variables influencing the prediction of the coefficient of discharge using dimensional analysis are expressed as:

$$C_m = f\left(F_r, \frac{H}{L}, \theta, \frac{H}{y_1}, \frac{y_1}{L}\right) \quad (5)$$

Table 1: Efficient dimensionless variables on the coefficient of discharge for 1-6 models

Number of the models	Variables (dimensionless)
First	$F_r.\frac{H}{L}.\theta.\frac{H}{y_1}.\frac{y_1}{L}$
Second	$F_r.\theta.\frac{H}{y_1}.\frac{y_1}{L}$
Third	$F_r.\frac{H}{L}.\frac{H}{y_1}.\frac{y_1}{L}$
Forth	$F_r.\frac{H}{L}.\theta.\frac{y_1}{L}$
Fifth	$F_r.\frac{H}{L}.\theta.\frac{H}{y_1}$
Sixth	$\frac{H}{L}.\theta.\frac{H}{y_1}.\frac{y_1}{L}$

where, F_r is the Froude number, H is the side weir step's height, L is the side weir's length, θ is the side weir's angle and y_1 is the side weir's flow depth upstream.

In this work, the functional form of Eq. 4 is evaluated in the experimental investigation. In the numerical study, six models are presented for estimating the coefficient of discharge based on Eq. 5. The data in Table 1 lists the dimensionless variables influencing the coefficient of discharge for all six models.

Experimental setup and procedure: The experimental setup included a main channel and a side-channel parallel to the main channel, as shown in Fig. 1. The trapezoidal cross-section main channel is 30 m long with a depth of 0.6 m. At the bottom, the main channel width is 1 m, with different bed slopes of 1-1000 and 1-3000. The rectangular side weir had a length of 4 m, a width of 0.85 m and was placed at the main channel's mid-section as indicated in Fig. 2. The distance between the side weir and both ends of the channel was 13 m.

The main channel's water supply came from a large 1.5 m deep feeding basin. The inlet discharge rates were measured by a sharp-crested rectangular weir. To measure the outlet discharge rates of the side weir, a calibrated rectangular weir at the end of the side channel was used. The measurements were taken with an accuracy of Lit/s. Three-point gauges with ±0.1 mm sensitivity were employed to measure the water depth. These gauges were placed at the side weir section and the centerline of the main channel. To be able to measure the depth of flow, a specific type of rail machine was used that was able to navigate in the x and y dimensions, as shown in Fig. 2. Pressures were measured using eight piezometers located on the centerline of the side weir. A sluice gate was installed at the end of the main channel to regulate the depth of flow as the downstream boundary condition. Nearly 300 experimental tests were performed for subcritical and

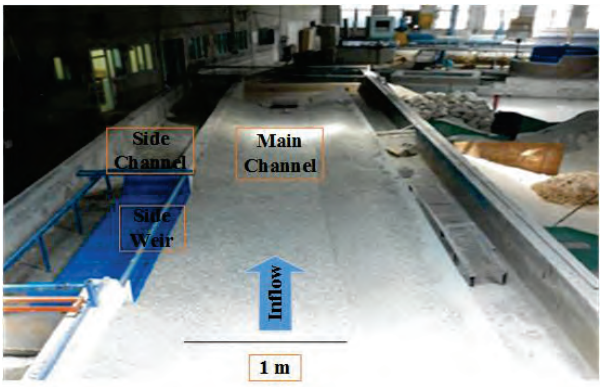

Fig. 1: A picture of the experimental setup

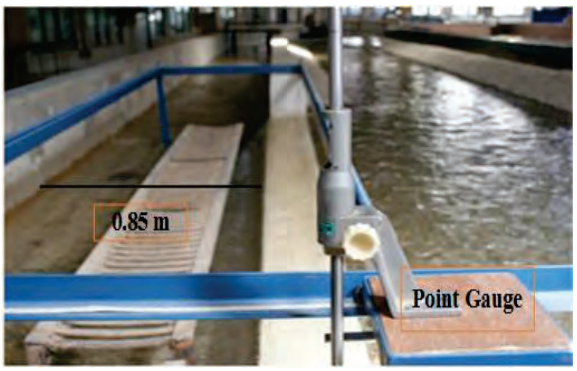

Fig. 2: Point gauge is mounted on the side weir

Table 2: Experimental parameters

Bed slope of main channel (S_0)	Froude number (F_{r1})	Height of weir (p) (cm)	Inlet discharge rate (Q_{in}) (lit/s)	Number of runs
1:1000	0.53-0.95	2-10	32-96	198
1:3000	0.53-0.95	2-10	32-96	99

stable flow conditions. The measurement results were compiled and used to develop a correlation for estimating the rectangular side weir's discharge coefficient. Table 2 shows the range of experimental parameters.

Numerical simulation

Computational fluid dynamic: The numerical simulations were carried out with the CFD software to estimate the side weir of broad crested shape's coefficient of discharge. The flow conditions and dimensions of the numerical model are the same as the aforementioned experimental model. The schematic of the simulated broad-crested side weir is illustrated in Fig. 3.

The equations employed in the simulations are the conservation of mass and momentum. The finite volume method was employed to model the multiphase flows. For a multiphase flow with components of velocities (u, v, w) along the cartesian coordinate axes (x, y, z), the governing Eq.:

$$Vf\frac{\partial \rho}{\partial t}+\frac{\partial}{\partial x}\left(\rho u A_x\right)+\frac{\partial}{\partial y}\left(\rho v A_y\right)+\frac{\partial}{\partial_z}\left(\rho w A_z\right)=0 \quad (6)$$

$$\begin{aligned}
&\frac{\partial u}{\partial t}+\frac{1}{VF}\left(uA_x\frac{\partial u}{\partial x}+vA_y\frac{\partial u}{\partial y}+wA_z\frac{\partial u}{\partial z}\right)=-\frac{1}{\rho}\frac{\partial \rho}{\partial x}+Gx+fx\\
&\frac{\partial v}{\partial t}+\frac{1}{VF}\left(uA_x\frac{\partial v}{\partial x}+vA_y\frac{\partial v}{\partial y}+wA_z\frac{\partial v}{\partial z}\right)=-\frac{1}{\rho}\frac{\partial \rho}{\partial y}+Gy+fy\\
&\frac{\partial w}{\partial t}+\frac{1}{VF}\left(uA_x\frac{\partial w}{\partial x}+vA_y\frac{\partial w}{\partial y}+wA_z\frac{\partial w}{\partial z}\right)=-\frac{1}{\rho}\frac{\partial \rho}{\partial z}+Gz+fz
\end{aligned} \quad (7)$$

Here, V_F is the open volume parameter for conducting the flow in the fast volume-reconstruction (favor) algorithm, which is specified in the next section. A_x is the open surface parameter conducting the flow along the x direction A_y and Az and represent the corresponding surface parameters along the y and z directions, respectively. In the conservation of

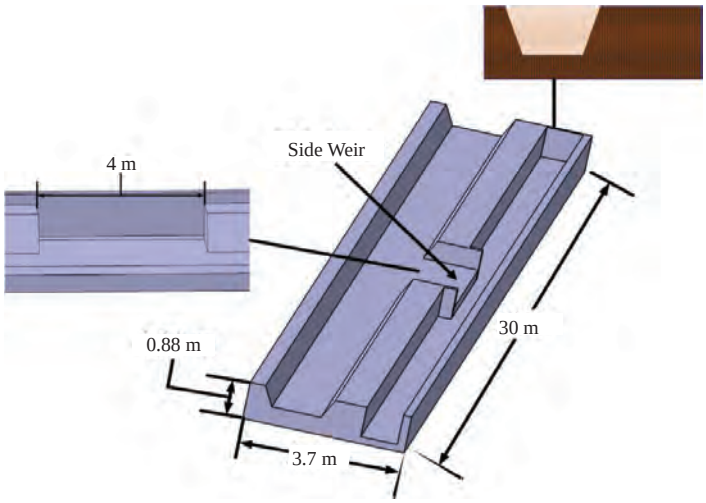

Fig. 3: Schematic of the simulated broad-crested side weir and the computational mesh

Table 3: Range of various parameters used in the simulation

Side weir's length (L) (m)	Side weir step's height (H) (cm)	Side weir's angle (θ) (°)	Number of simulations
3, 4 and 5	12.62, 25.24 and 37.86	10, 20, 30, 45 and 60	45

momentum equations, ρ is the density of the fluid and (Gx, Gy, Gz) are the components of body acceleration. In these equations, (fx, fy, fz) are the effects of both molecular viscosity and viscosity because of turbulence. Generally, two-equation models are employed in hydraulics for turbulence modelling. The RNG k-ε three-dimensional turbulence model was used in the present study to solve the Reynolds-averaged equations[31].

To determine the appropriate geometry in the finite volume method, the surface/volume elements expressing obstacles were employed in the FAVOR algorithm. In this algorithm, values between 0 (air) and 1 (water) are assigned to phases, i.e., water and air in the computational cell domains. If water fills the entire cell, then the surface/volume element is given the value of 1. The Volume of Fluid (VOF) algorithm can determine the free surface of the flow. The numerical simulations were conducted using the VOF method with open channel options, which allows for defining free surface levels and velocities (and so froude numbers) at the inlet boundary. Modified high-resolution interface capturing (HRIC) method with an implicit scheme was employed to achieve a sharp interface and greater accuracy between phases. To simulate the face fluxes for all elements, the implicit scheme employed a standard finite-difference interpolation scheme as follows:

$$\frac{a_q^{n+1}\rho_q^{n+1} - a_q^n\rho_q^n}{\Delta t}V + \sum_f\left(\rho_q^{n+1}U_f^{n+1}a_{q,f}^{n+1}\right) = \left[S_{aq} + \sum_{p=1}^{n}\left(m_{pq} - m_{qp}\right)\right]V \quad (8)$$

In which n+1 is the superscript of the current time step, is the superscript of the previous time step, $a_{q,f}$ is the face value of the th volume fraction estimated from the modified HRIC method, V is cell volume, U_f is volume flux from the face. The time step size was 0.01s in the solutions. To obtain the iteration convergence for the unsteady cases, the solutions continue until the residuals drop at least three order magnitudes for each equation.

In the numerical simulations, three specific geometry parameters, side weir length (L), side weir step height (H) and side weir angle (θ) are changed and various parameter ranges are presented in Table 3. These changes in geometry parameters and boundary conditions are shown in Fig. 4. The inlet boundary condition for the main channel was a specified volume flow rate. The outflow condition was considered at the end of the side and main channels. Furthermore, a pressure outlet boundary condition was specified at the top of the domain. Other boundaries were considered as a wall boundary condition.

As shown in Fig. 5, several structured meshes were used to achieve a reliable accuracy and convergence of the numerical solution. Roache[32] recommended that the grid refinement factor should be set to a value of approximately 10%. For grid study, simulations are performed for the flow rate of 52 lit/s in the main channel with a slop of 0.001 using 10^6, 4×10^6, 75×10^5 and 9×10^6 cells. The flow depth at a point 13 meters from the beginning of the main channel is presented in Fig. 5. This figure shows that the simulation results with more than 75×10^5 grids are independent of the grid size. The number of elements in the x, y and z directions

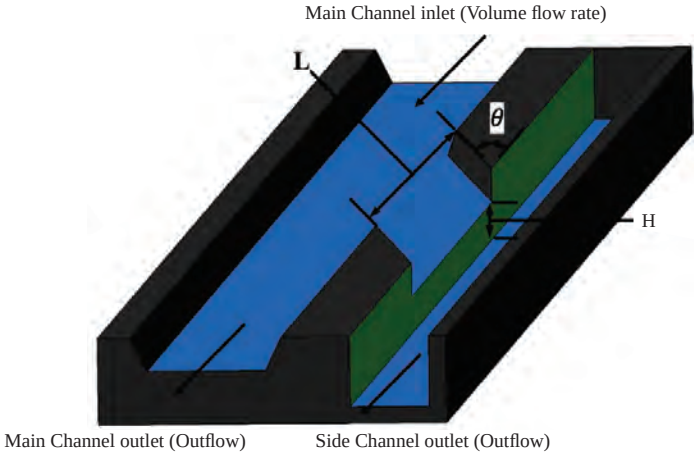

Fig. 4: Three-dimensional sketch, main geometric variables of a broad-crested side weir and boundary conditions

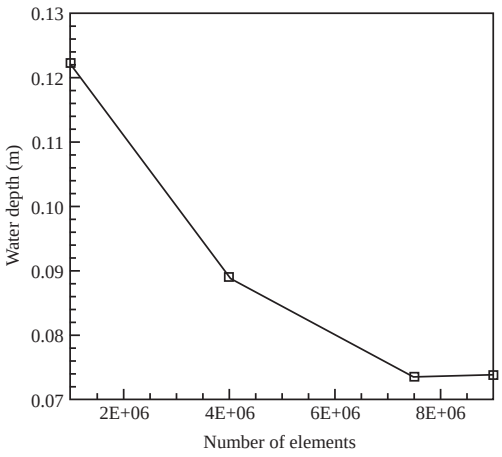

Fig. 5: Grid independence tests (water depth in the centerline of the main channel for different grid numbers, Q_{in} = 52 Lit/s, bed slope of 0.001)

is 1000, 150 and 50, respectively, with the element sizes of 0.03 m in the x-direction, 0.024 m in the y-direction and 0.016 m for z-direction.

Gene expression programming: Gene expression programming (GEP), as a novel method based on Genetic Programming (GP), was first developed by Ferreira[33]. GEP, alongside the GP and the genetic algorithm (GA), are transformative methods capable of establishing programs of complicated nature. The GEP technique is similar to the evolution theory of Darwin, in which natural selection research methods and optimization are applied to attain excellence. Various computer programs, which are models of quasi-mathematical nature and established upon the specified function of fitness to resolve the issue of evolution, are applied to develop the process of GEP.

Commonly, GEP comprises five basic elements, the terminal set, fitness function, control parameters, function set and termination conditions[34]. To show the technique used for problem-solving, GEP utilizes string characters of fixed-length parse trees shapes of several sizes and forms. Expression trees (ETs) is the name given to these trees. One significant benefit of the GEP is its ordinary variety in genetics, whereby employing genetic operators of various kinds, GEP takes action at various levels of the chromosome. Also, the mutagenic character, a remarkable aspect of GEP, guides to a program with a convened nature consisting of subprograms to attain an optimal solution. Several symbols are assigned to all of the available genes in GEP. The genes can be employed as part of the terminal set while their length is permanent, for example (Y. X. Z. 5) and the determined set of function, for instance (+. ×. -. /. √). All functions must be suitable to get any data, reinstate a function, or be taken into account by a terminal. A typical gene of GEP with a terminal function presumed as mentioned is represented as the following:

$$+.\times.\surd.\,X.-.+.\times.\,Y.\,X.\,Z.\,5.\,Y.\,Z. \quad (9)$$

Here, 5 is a constant and Z, Y and X are parameters. K-notation is the given name to the expression of Eq. 9[28]. The expression tree diagram can be one of the representatives of the K-notation.

In this effort, based on GEP, a model is introduced employing optimization programming software. Next, the coefficient of discharge modeling for side weirs in channels with trapezoidal shape is presented. First, the function of

Table 4: Values of various variables in the practical gene expression programming (GEP)

Parameters	Setting
General	
Chromosomes' quantity	45
Gene	3
Size of the head	10
Rate of mutation	0.01
Rate of inversion	0.1
Genetic operators	
Rate of IS transposition	0.1
Rate of RIS transposition	0.1
Rate of one-point recombination	0.3
Two-point recombination	0.3
Recombination of gene	0.1
Transposition of gene	0.1
Generations' quantity	300.000
Tires' quantity	3
Increase in complexity	
Maximum complexity	5

Table 5: Functions employed for GEP model

Name of the functions	Label in expression tree	Name of the function	Label in expression tree
Multiplication	*	Inverse	Inv
Addition	+	x to the power of 2	X^2
Division	/	Arctangent	$\tan^{-1}$
Subtraction	-	hyperbolic tangent	tanh
Exponential	Exp	Complement	Not
Natural logarithm	Ln		

fitness for this particular problem must be specified. In the present study, RMSE (root mean squared error) is utilized as proposed by Shiri and Kisi[35]. The function of fitness of the RMSE (E_i) for each computer program is expressed as:

$$E_i = \sqrt{\frac{\sum_{j=1}^{n}\left(P_{ij} - T_j\right)^2}{n}} \quad (10)$$

where, T_j is the fitness case target value j, P_{ij} is the individual program's anticipated value employing GEP for the fitness case j and n represents the samples' total number. The most effective answer is achieved when T_j the P_{ij} and values are equal to each other consequently, $E_i = 0$. To evaluate the f_i function or the fitness of the individual computer program i, a formula is utilized. That is:

$$f_i = \frac{1000}{1 + E_i} \quad (11)$$

As illustrated in 0-1000 range, the equation conversions and the most effective result is obtained when $E_i = 0$ and thus $f_i = 1000$[36]. Subsequently, when the fitness function is defined, the function set (F) and the terminal set (T) are determined. Concerning the present investigation, the T comprises $\left(C_m.F_r.\frac{H}{L}.\theta.\frac{H}{y_1}.\frac{y_1}{L}\right)$ and the F is comprised of main arithmetic operators (+. -. ×. /) and (4Rt. 5Rt. X2. X3. Ln. Sin. Arctan). Next, the architecture of the chromosome must be specified. Corresponding to the expressed values in the literature[33,36,37,38], the length of the head is assumed to be 10. Various genes' linking function regarded in this work is also due to the good efficiency of this function in the latest research[24]. In the end, different operators of genetic type should be specified. The values dependent on these procedures are presented in Table 4. Also, in this study, GEP functions used for optimization are represented in Table 5.

RESULTS AND DISCUSSION

Experimental results: The flow over a rectangular broad-crested side weir in the trapezoidal channel is studied and a new correlation for the corresponding discharge coefficient as a function of non-dimensional variables defined in Eq. 4 was developed. As noted before, the discharge coefficient, C_m is a function of several dimensionless groups, including froude number, F_{r1} channel slope and the geometry of the weir and the channel, p/y_1 ,y_1/b . To measure the effect of each of these variables, several experiments are performed and the influence of each parameter is determined. Figure 6 shows the variation of measured values of C_m against F_{r1} for different values of S_0. The values of p/y_1 and y_1/B are fixed as 1m, 1.25 and 0.1, respectively. The C_m of side weir with S_0 = 1-1000 was 1.3-1.7 times higher than that of side weir's with S_0 = 1-3000. This figure shows that by increasing flow velocity with changing the bed slope, the discharge coefficient

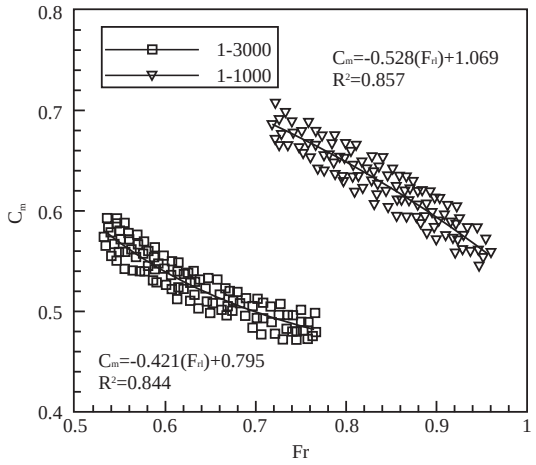

Fig. 6: Variation of measured C_m versus for various F_{r1} values of bed slope S_0

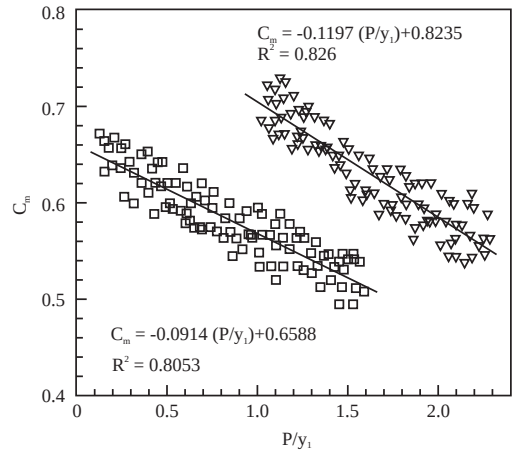

Fig. 7: Variation of measured C_m versus $\frac{p}{y_1}$ for various values of bed slope S_0

Table 6: Different hydraulic/geometric variables of broad-crested side weir

Hydraulic and geometric variables	Values
F_{r1}	0.53-0.95
S_0	1-1000 and 1-3000
p/y_1	0.13-2.22
y_1/B	0.045-0.15

increases. Figure 6 also shows that with the increase of the upstream Froude number, the values decrease. This result means that higher C_m values are achieved at lower upstream Froude numbers due to the decrease of flow velocity and increase of depth of flow.

In Fig. 7, the values of C_m are plotted against the ratio of weir height to water depth, $\frac{p}{y_1}$, for different bed slopes. The values of $\frac{y_1}{B}$ and F_{r1} are considered as 0.1 and 0.75, respectively. It is seen that C_m values decrease when $\frac{p}{y_1}$ ratio increases. An increase in the bed slope of the main channel increased the discharge coefficient. In addition, The side weir's coefficient of discharge variation in terms of the ratio of the upstream flow depth to the main channel width $\frac{y_1}{B}$ can be seen in Fig. 8 for various bed slopes. The values of $\frac{p}{y_1}$ and F_{r1} are fixed as 1.25 and 0.75, respectively. It is seen that C_m values increase whenever the $\frac{y_1}{B}$ ratio increases. Since the channel width is constant, the water depth increases and causes the lateral discharge to increase as well. The broad-crested side weirs of different hydraulic and geometric variables (F_{r1}, S_0, $\frac{p}{y_1}$, $\frac{y_1}{B}$) were studied under various conditions, as listed in Table 6.

As expressed in previous studies, the upstream Froude number is the key influential factor affecting the discharge coefficient. Therefore, all the obtained experimental data was used and regression in different bed slopes for obtaining the best fit which is given as:

$$C_m = -0.1479+0.0446\left(\frac{p}{y_1}\right)^{-3.97} + 0.711\left(F_{r1}\right)^{-0.431} +0.0039\left(\frac{y_1}{B}\right)^{0.128} \left(S_0 = 1-1000\right) \quad (12)$$

$$C_m = -0.1923+0.00212\left(\frac{p}{y_1}\right)^{3.24} + 0.436\left(F_{r1}\right)^{-0.404} +0.32\left(\frac{y_1}{B}\right)^{0.229} \left(S_0 = 1-3000\right) \quad (13)$$

Figure 9 compares the measured values of C_m against the computed values C_m across the entire range of the included parameters. As can be seen from Fig. 9, Eq. 12 provides a reasonably accurate estimate of the experimental data.

The statistical indices Root Mean Square Error (RMSE), Mean Absolute Relative Error (MARE), Scatter Index (SI) and BIAS methods are employed to investigate the accuracy of the used models. They are defined as:

$$RMSE = \sqrt{\frac{\sum_{i=1}^{n}\left(C_{m(Predicted)_i} - C_{m(observed)_i}\right)^2}{n}} \quad (14)$$

$$MARE = \frac{1}{n}\sum_{i=1}^{n}\left(\frac{\left|C_{m(Predicted)_i} - C_{m(observed)_i}\right|}{n}\right) \quad (15)$$

$$SI = \frac{RMSE}{\overline{C}_{m(observed)_i}} \quad (16)$$

$$BIAS = \frac{1}{n}\sum_{i=1}^{n}\left(C_{m(Predicted)_i} - C_{m(observed)_i}\right) \quad (17)$$

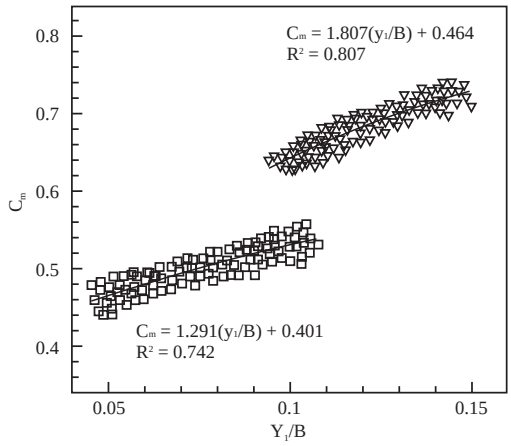

Fig. 8: Variation of measured C_m versus $\frac{y_1}{B}$ for various values of bed slope S_0

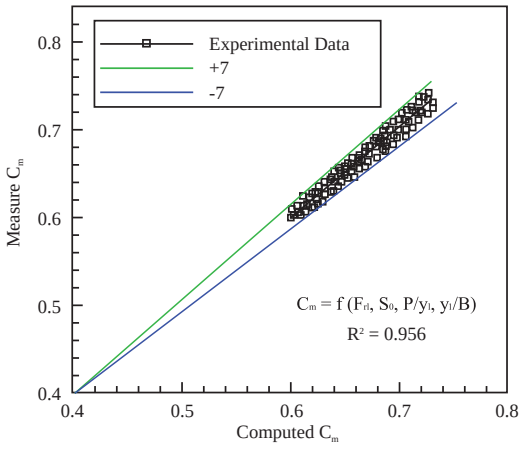

Fig. 9: Comparison of the computed and measured values of C_m

Here, $C_{m(predicted)i}$-$C_{m(predicted)i}$-$\overline{C}_{m(observd)i}$ and are, respectively, the experimental discharge coefficient, the predicted coefficient of discharge, the average coefficient of discharge and the number of measurements. The statistical indices RMSE, MARE, SI and BIAS for two different bed slopes are shown in Table 7.

As noted before, the bed slope and the Froude number have major effects. As already mentioned, due to the experimental results, the purpose of this work was to analyze the hydraulic performance of the rectangular broad crested side weir based on limited parameters such as F_{r1}. S_0. $\frac{p}{y_1}$. and $\frac{y_1}{B}$. Hence, different hydraulic and geometry parameters are discussed in the following sections using numerical methods.

Numerical results

Validation: The results of the numerical simulations were validated using the experimental data. The comparison of the simulation and experimental surface profiles of water through the trapezoidal main channel centerline for Q_{in} = 110 Lit/s, bed slope of 1-1000, side weir length of 4 m and height step of 12.62 cm as shown in Fig. 10. It is seen that the flow depth in the main channel decreased significantly due to the side weir. In addition, decreasing the flow depth in the main channel caused an ascending trend in the flow depth along the side weir length. Figure 10 indicates that the numerical results are in good agreement with the experimental data. Furthermore, the percent error of the numerical results compared with the experimental data was within a ±6% error limit, which is acceptable.

Water surface profile: The Water surface profile is an essential variable describing flow patterns in an open channel. Water levels along the side weir and main channel lengths are simulated and the water surface profiles are obtained. These simulations were performed for the domain that is 4 m before the upstream edge of the side weir to 2 m after the downstream of the side weir for an inlet discharge rate of 52 Lit/s and various bed slopes. Along the centerline, Water surface profiles for flow over the main channel and the side weir for different bed slopes and an inlet discharge rate of 52 Lit/s are presented in Fig. 11a-b, respectively. The data in Fig. 11a shows the water profile along the 10 m length in the middle-point of the main channel. The data in Fig. 11a shows a sharp decrease in the water level at the start of the side weir in the main channel. Namaee *et al.*[16] have investigated the flow behaviour along the side weir in a trapezoidal channel. Namaee *et al.*[16] have reported the presence of secondary flow as the reason for this behaviour. As seen in Fig. 11b, free surface levels gradually rose towards the downstream end of the side weir due to the secondary flow. The secondary flow disperses main channel flow energy and causes a rise in water level along the side weir length. Also, with an increase in the bed slope, the mainstream velocity in the entire flow regime increases accordingly. Therefore, the water surface level of both the main and side channels is increased.

The velocity field: In common side weirs that are located perpendicular to the flow direction, the passing flow is considered approximately two-dimensional. Azimi *et al.*[39] have

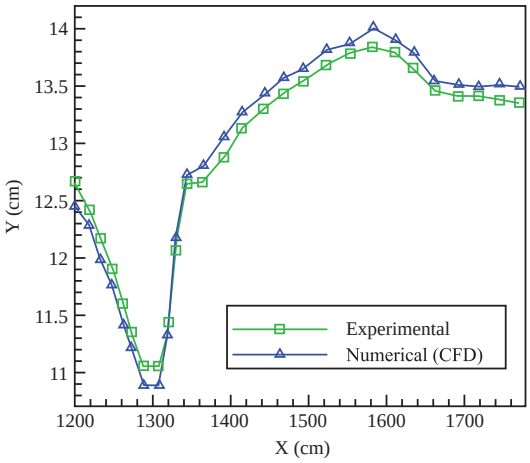

Fig. 10: Experimental and numerical water surface profile through the centerline of the main channel for Qin = 110 Lit/s, bed slope of 1-1000, side weir of 4 m length and height step of 12.62 cm

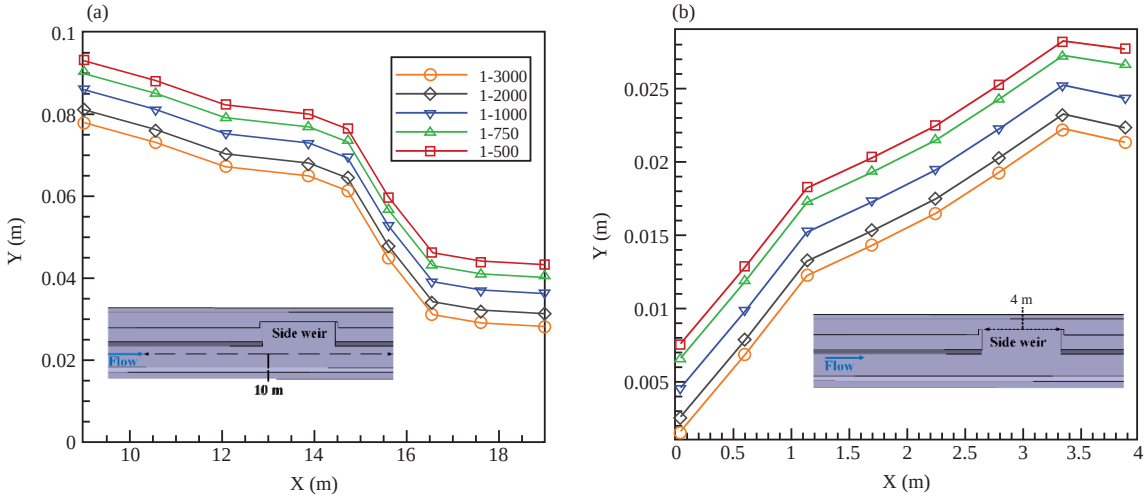

Fig. 11(a-b): Flow profile for different bed slopes and inlet discharge rate of 52 Lit/s, (a) Main channel and (b) Side weir

Table 7: Statistical indices results

Bed slope (S_0)	RMSE	MARE	SI	BIAS
1-1000	0.0158	0.0341	0.0398	0.01
1-3000	0.0395	0.0687	0.074	0.022

investigated the longitudinal velocity distribution passing over typical side weirs in circular channels. They found that the maximum velocity occurs near the side weir crest. Bagheri and Heidarpour[5], in their studies, indicated that the maximum longitudinal velocity happens at the upstream end of the side weir. Figure 12 shows the longitudinal velocity contours in the main channel and on the side weir for an inlet discharge rate of 52 Lit/s and bed slope of 1-1000. This figure shows that the maximum longitudinal velocity occurs near the downstream end of the side weir and the free surface. Then immediately after the peak, the velocity drops and reaches its lowest value. In Fig. 12, the stagnation zone near the right side wall of the side channel downstream of the side weir is seen. The stagnation region was also seen in the experimental study. In addition, Fig. 12 shows the secondary flow at the cross-section of the main channel due to the lateral flow presented by Y-component velocity vectors. The secondary flow related to the mean kinetic energy of lateral motion in the main channel significantly influences the discharge efficiency. Streamlines are also diverted to the side weir outlet due to the

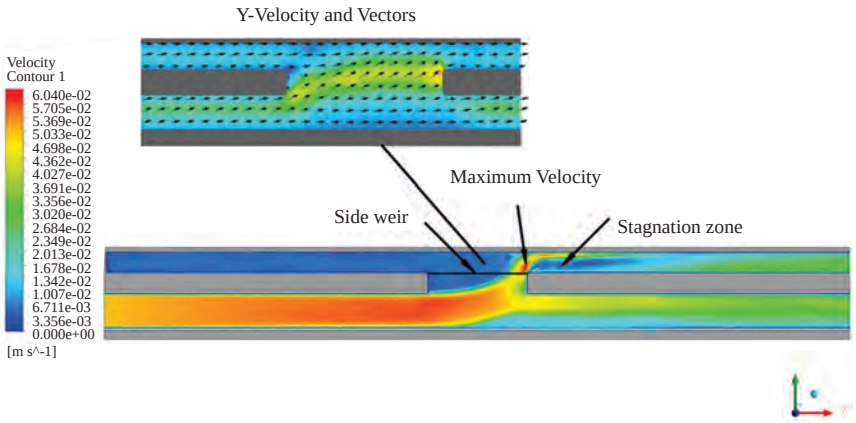

Fig. 12: Simulated longitudinal and lateral velocity contours in the main channel and side weir for Q_{in} = 52 Lit/s, S_0 = 1-1000

secondary flow. Emiroglu *et al.*[20] suggested that the intensity of the secondary flow is related to the froude number, the location of the side weir and the height of the weir crest.

Discharge rate of the side weir: The key problem in practice is determining the discharge behaviour of a side weir, which is primarily described by the discharge coefficient. The average specific energy difference between the downstream and upstream ends of the side weir must be approximately less than 5%[8] to use the De Marchi equation, which is based on a constant energy theory. Thus, the following analysis is performed using the assumption of constant specific energy. The effect of bed slope on the outlet discharge rate of broad crested side weir is calculated numerically in Fig. 13. It is seen that increasing the bed slope of the channel increases the side weir discharge rate in the side weir.

Statistical indices and superior geometry: To assess the correctness of 1-6 models in the Table 1, RMSE, MARE, R^2 (coefficient of correlation), SI and BIAS are evaluated:

$$RMSE = \sqrt{\frac{\sum_{i=1}^{n}\left(C_{m(GEP)_i} - C_{m(EXP)_i}\right)^2}{n}} \quad (18)$$

$$MARE = \frac{1}{n}\sum_{i=1}^{n}\left(\frac{\left|C_{m(GEP)_i} - C_{m(EXP)_i}\right|}{C_{m(EXP)_i}}\right) \quad (19)$$

$$R^2 = \frac{\left(n\sum_{i=1}^{n} C_{m(GEP)_i} C_{m(EXP)_i} - \sum_{i=1}^{n} C_{m(GEP)_i}\sum_{i=1}^{n} C_{m(EXP)_i}\right)^2}{\left(n\sum_{i=1}^{n}\left(C_{m(GEP)_i}\right)^2 - \sum_{i=1}^{n}\left(C_{m(GEP)_i}\right)^2\right)\left(n\sum_{i=1}^{n}\left(C_{m(EXP)_i}\right)^2 - \sum_{i=1}^{n}\left(C_{m(EXP)_i}\right)^2\right)} \quad (20)$$

$$SI = \frac{RMSE}{\overline{C}_{m(EXP)_i}} \quad (21)$$

$$BIAS = \frac{1}{n}\sum_{i=1}^{n}\left(C_{m(GEP)_i} - C_{m(EXP)_i}\right) \quad (22)$$

Here, $C_m(GEP)_i$, $C_m(GEP)_i$, $\overline{C}_m(GEP)_i$ and are the coefficient of discharge estimated by gene expression programming, the coefficient of discharge estimated in the experiments (EXP), the average experimental discharge coefficient and the total number of experimental tests, respectively. The statistical indices MARE, RMSE, R^2, SI and BIAS indicate the errors between the experimental tests and GEP coefficients of discharge. The RMSE index only shows a root mean square error between the model prediction and experiment[8]. Thus, the models should be assessed employing threshold statistics and indices of other kinds[40,41]. The TS_x index indicates the distribution of error in the amounts estimated by each of the models for X% of anticipations. This variable is specified for different mean absolute relative error amounts. TS_x index's amount for X% of the anticipations is provided as the following:

$$TS_x = \frac{Y_x}{n} \times 100 \quad (23)$$

In the equation above, Y_x represents the predicted quantities for all of the MAREs lower than X% of the total amount of data. The presented statistical indices are described in references[42,43].

The MARE, RMSE, BIAS and SI values obtained for the first model are, respectively, 0.025, 0.01, 0.013 and 0.036. The first model is a function of the side weirs upstream Froude number

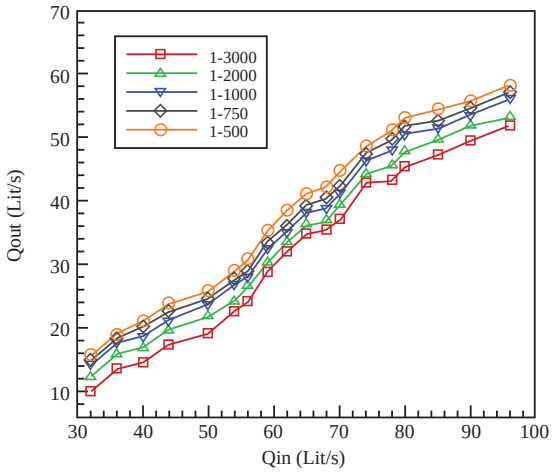

Fig. 13: Calculated side weir discharge rate for broad-crested rectangular side weir for different bed slopes

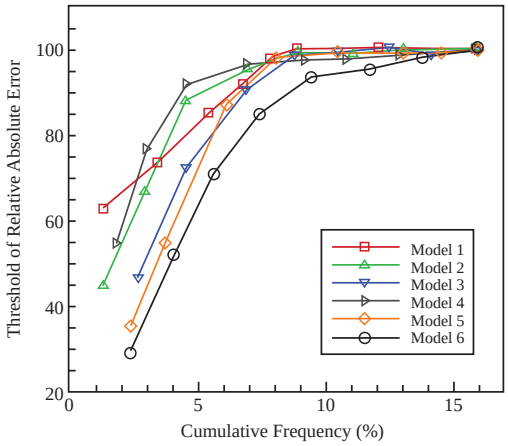

Fig. 14: Error distributions of different models

(F_r), the height of side weir step to side weir length ratio $\left(\frac{H}{L}\right)$, side weir angle (θ), side weir's flow depth upstream to the height of side weir step ratio $\left(\frac{H}{y_1}\right)$ and the side weir flow depth upstream to the length of side weir ratio $\left(\frac{y_1}{L}\right)$. These are the variables that affect the coefficient of discharge. Based on the error distribution study as indicated in Fig. 14, it is clear that 88.5% of data for the first model have an error of less than 5% and just 11.5% have an error of 5-10%. Posited by error distribution, no discharge coefficient has more than 10% error.

The second model is a function of F_r, θ, $\frac{H}{y_1}$ and $\frac{y_1}{L}$ and the MARE and RMSE values calculated for the second model are 0.029 and 0.012, respectively. The BIAS and SI indices estimated for the second model are 0.010 and 0.034, respectively. In the mentioned model, 10.5% of data have an error of 5-10%, while 85.3% of the error is below 5%. In addition, 4.2% of the second model data have an error of more than 10%.

For the third model, the side weir discharge coefficient is a function of $F_r.\frac{H}{L}.\frac{H}{y_1}$ and $\frac{H}{y_1}$, in which MARE and RMSE values of 0.032 and 0.013, respectively, were obtained. The computed BIAS and SI values of the third model are 0.012 and 0.035, respectively. In the third model, 15.3% of data have an error between 5% and 10% and 84.7% of data have an error below 5%. Furthermore, in the third model, all of the discharge coefficients have an error of less than 10%.

For the fourth model, MARE and RMSE are 0.035 and 0.013, respectively. The computed BIAS and SI for the mentioned model are 0.010 and 0.029, respectively. The fourth model's coefficient of discharge is a function of $F_r.\frac{H}{L}.\theta$ and $\frac{y_1}{L}$ and a prediction error of 5-10% in just 10.72% of the data is seen, while the error of 86.28% of data is lower than 5%. In addition, the error of 3% of the data of the fourth model is less than 10%.

The fifth model's MARE and RMSE values are 0.033 and 0.015, respectively. The BIAS and SI of this model are 0.012 and 0.04, respectively, while 70% of data have an error of lower than 5%. Finally, the prediction error of all of the discharge coefficients is less than 10%. $F_r.\frac{H}{L}.\theta$ and $\frac{H}{y_1}$ are the variables that this model is a function of. Amongst all models, the model with maximum error is the sixth model (MARE = 0.039, RMSE = 0.020, SI = 0.045 and BIAS = 0.015). For the sixth model, 5.15% of the estimated discharge coefficients have an error of more than 10 and 32.5% have an error between 5% to 10. The error distributions for different models are shown in Fig. 14. Also, the MARE, RMSE, BIAS, SI and R^2 values for all models are presented in Table 8.

Investigating the modelling results for the coefficient of discharge of a side weir in a channel of trapezoidal shape using GEP, the first model is the most suitable. The correlation given by Eq. 20 is developed using the results of the coefficient of discharge of the side weir for the first model. In addition, according to the experimental results, the GEP results demonstrated that the discharge coefficient of broad-crested rectangular side weir is improved. The optimized geometry model is a 5 m in length side weir step with a height of 37.86 cm and a side weir angle of 60°:

$$C_m = \arctan\left[-0.269\tanh\left(\frac{y_1}{L}\right)\times\left(\frac{H}{y_1}\right)\times\arctan\left(F_r\right)\right]+\left[-0.266\left(\log F_r\right)\times\left(\left(\frac{H}{L}+\frac{y_1}{L}\right)+\log 0.966\right)\right]+\left[\tanh\left(\arctan\left(\arctan\left(\left(F_r\right)^{10}\times\left(\frac{H}{y_1}\right)^2\right)\right)\right)\right]+\left[0.0922-\left(\left(\frac{H}{L}\right)\times\left(\tan\theta^2\times F_r\right)-\left(\frac{H}{y_1}\right)^2\right)\right]+\left[-4.13\log F_r\times\left(\frac{H}{L}\right)\right] \quad (24)$$

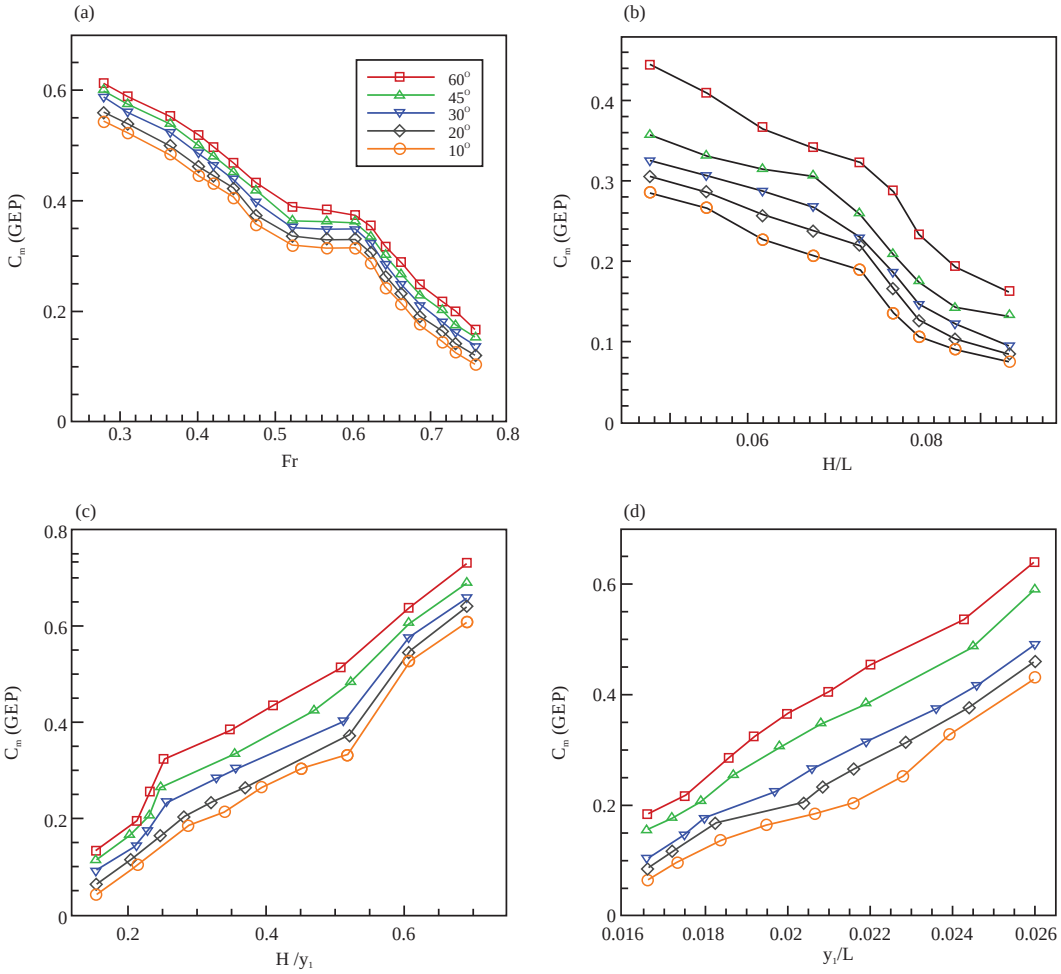

Fig. 15(a-d): Comparison of the discharge coefficient vs- $F_r.\frac{H}{L}.\frac{H}{y_1}.\frac{y_1}{L}$ attained along the side weir for various side weir angles

Table 8: Statistical indices and error distribution for different models

Statistical indices models	MARE	RMSE	BIAS	SI	R^2	Error≤5%
1	0.025	0.01	0.013	0.036	0.964	88.5
2	0.029	0.012	0.01	0.034	0.919	85.3
3	0.032	0.013	0.012	0.035	0.892	84.7
4	0.035	0.013	0.01	0.029	0.864	86.28
5	0.033	0.015	0.012	0.04	0.837	70
6	0.039	0.02	0.015	0.045	0.812	62.35

As noted before, C_m is a function of parameters $F_r.\frac{H}{L}.\theta.\frac{H}{y_1}.\frac{y_1}{L}$. To study the influence of side weir angle, different angles such as 10°, 20°, 30°, 45° and 60° are considered. It is observable that an increase in θ increases in the C_m values. As indicated in Fig. 15a, increasing side weirs' angle increases the coefficient of discharge along the side weir also, it is deduced that the coefficient of discharge reduces with the Froude number's increase along the length of the side weir. Especially, higher values of C_m are attained at a Froude number of low upstream owing to the growth of the depth of the flow and reduction of the velocity of the flow. Variation of C_m against various $\frac{H}{L}$ ratios are depicted in Fig. 15b. It is seen that, an increase in the $\frac{H}{L}$ ratio results in an increase in the values of the coefficient of discharge. An increase in the values of the coefficient of discharge is probably due to the secondary flows crested by a side flow. To investigate the influence of the ratio of $\frac{H}{y_1}$ on the coefficient of discharge, the values of C_m are plotted against $\frac{H}{y_1}$ for various side weir angles in Fig. 15c. It is concluded from these plots that the coefficient of discharge values increase with an increase in $\frac{H}{y_1}$. The variation of C_m against the ratio of the depth of the upstream side weir flow to the length of the side weir $\frac{y_1}{L}$ also can be seen from Fig. 15d. This figure

shows an increase in $\frac{y_1}{L}$ ratio results in an increase in the values of coefficient of discharge. The side discharge increases due to the increase in the depth of the water. As seen from Fig. 15c-d, the discharge coefficient is increased with an increase in the side weir angle.

CONCLUSION

In the present work, the experimental study, CFD and GEP simulations were used to analyze the hydraulic characteristics of the rectangular broad-crested side weir in the trapezoidal channel. The analysis of the experimental data shows that the discharge coefficient of a broad-crested rectangular side weir is a function of $F_{r1}, S_0, \frac{p}{y_1}$, and $\frac{y_1}{B}$ and a new correlation for the discharge coefficient was developed. In the CFD and GEP simulations, the dimensionless variables $F_r, \frac{H}{L}, \theta, \frac{H}{y_1}$ and $\frac{y_1}{L}$ and six models were employed to predict the discharge coefficient. Therefore, the most appropriate correlation was also identified. Finally, based on CFD and GEP simulations, a practical discharge coefficient for rectangular broad-crested side weir is introduced for hydraulic applications.

SIGNIFICANCE STATEMENT

The presented comprehensive investigation evaluated the major hydraulic parameters of flow around the rectangular broad-crested side weir in the trapezoidal-type main channel that can be beneficial for developing novel discharge coefficients. The results of this study help the researcher uncover the critical area of designing an optimum rectangular side weir that is of significant interest in many hydraulic and irrigation management projects.

REFERENCES

1. Kumar, S., Z. Ahmad and T. Mansoor, 2011. A new approach to improve the discharging capacity of sharp-crested triangular plan form weirs. Flow Meas. Instrum., 22: 175-180.
2. Abbasi, S., S. Fatemi, A. Ghaderi and S.D. Francesco, 2021. The effect of geometric parameters of the antivortex on a triangular labyrinth side weir. Water, Vol. 13. 10.3390/w13010014.
3. Granata, F., G. de Marinis, R. Gargano ans C. Tricarico, 2013. Novel approach for side weirs in supercritical flow. J. Irrig. Drain Eng., 139: 672-679.
4. Emiroglu, M.E., H. Agaccioglu and N. Kaya, 2011. Discharging capacity of rectangular side weirs in straight open channels. Flow Meas. Instrum., 22: 319-330.
5. Bagheri, S. and M. Heidarpour, 2012. Characteristics of flow over rectangular sharp-crested side weirs. J. Irrig. Drain. Eng., 138: 541-547.
6. Shariq, A., A. Hussain and M.A. Ansari, 2018. Lateral flow through the sharp crested side rectangular weirs in open channels. Flow Meas. Instrum., 59: 8-17.
7. Hussain, A., Z. Ahmad and G.L. Asawa, 2011. Flow through sharp-crested rectangular side orifices under free flow condition in open channels. Agric. Water Manage., 98: 1536-1544.
8. Granata, F. and G. de Marinis, 2017. Machine learning methods for wastewater hydraulics. Flow Meas. Instrum., 57: 1-9.
9. Maranzoni, A., M. Pilotti and M. Tomirotti, 2017. Experimental and numerical analysis of side weir flows in a converging channel. J. Hydraul. Eng., Vol. 143. 10.1061/(ASCE)HY.1943-7900.0001296.
10. S.M. Borghei and A. Parvaneh, 2011. Discharge characteristics of a modified oblique side weir in subcritical flow. Flow Meas. Instrum., 22: 370-376.
11. Azimi, H., S. Shabanlou, I. Ebtehaj and H. Bonakdari, 2016. Discharge coefficient of rectangular side weirs on circular channels. Int. J. Nonlinear Sci. Numer. Simul., 17: 391-399.
12. Afshar, H. and S.H. Hosein, 2013. Experimental and 3-D numerical simulation of flow over a rectangular broad-crested weir. Int. J. Eng. Adv. Technol., 2: 214-219.
13. Azimi, H., H. Bonakdari and I. Ebtehaj, 2019. Design of radial basis function-based support vector regression in predicting the discharge coefficient of a side weir in a trapezoidal channel. Appl. Water, Sci., Vol. 9. 10.1007/s13201-019-0961-5.
14. Nezami, F., D. Farsadizadeh and M.A. Nekooie, 2015. Discharge coefficient for trapezoidal side weir. Alexandria Eng. J., 54: 595-605.
15. Vatankhah, A.R., 2012. Briefing: Water surface profile over side weir in a trapezoidal channel. Proc. Inst. Civ. Eng. Water Manage., 165: 247-252.
16. Namaee, M.R., M.S. Jalaledini, M. Habibi, S.R.S. Yazdi and M.G. Azar, 2013. Discharge coefficient of a broad crested side weir in an Earthen channel. Water Supply, 13: 166-177.
17. Ghorbannia, D. and A. Eghbalzadeh, 2018. Numerical study of the effect of length change on the flow pattern around a side weir in a converging channel. Acta Mechanica, 229: 4101-4111.
18. Bilhan, O., M.E. Emiroglu and O. Kisi, 2010. Application of two different neural network techniques to lateral outflow over rectangular side weirs located on a straight channel. Adv. Eng. Software, 41: 831-837.
19. Emiroglu, M.E. and N. Kaya, 2010. Discharge coefficient for trapezoidal labyrinth side weir in subcritical flow. Water Resour. Manage., 25: 1037-1058.

20. Emiroglu, M.E., M.C. Aydin and N. Kaya, 2014. Discharge characteristics of a trapezoidal labyrinth side weir with one and two cycles in subcritical flow. J. Irrig. Drain. Eng., Vol. 140. 10.1061/(ASCE)IR.1943-4774.0000709.
21. Aydin, M.C. and M.E. Emiroglu, 2016. Numerical analysis of subcritical flow over two-cycle trapezoidal labyrinth side weir. Flow Meas. Instrum., 48: 20-28.
22. Wang, Y., W. Wang, X. Hu and F. Liu, 2018. Experimental and numerical research on trapezoidal sharp-crested side weirs. Flow Meas. Instrum., 64: 83-89.
23. Gopakumar, R. and P.P. Mujumdar, 2008. A fuzzy dynamic wave routing model. Hydrol. Proc., 22: 1564-1572.
24. Ebtehaj, I., H. Bonakdari, A.H. Zaji, H. Azimi and A. Sharifi, 2015. Gene expression programming to predict the discharge coefficient in rectangular side weirs. Appl. Soft Comput., 35: 618-628.
25. Khoshbin, F., H. Bonakdari, S.H.A. Talesh, I. Ebtehaj, A.H. Zaji and H. Azimi, 2016. Adaptive neuro-fuzzy inference system multi-objective optimization using the genetic algorithm/singular value decomposition method for modelling the discharge coefficient in rectangular sharp-crested side weirs. Eng. Optim., 48: 933-948.
26. Jahanpanah, E., P. Khosravinia, H. Sanikhani and O. Kisi, 2019. Estimation of discharge with free overfall in rectangular channel using artificial intelligence models. Flow Meas. Instrum., 67: 118-130.
27. Azimi, H., H. Bonakdari and I. Ebtehaj, 2017. Sensitivity analysis of the factors affecting the discharge capacity of side weirs in trapezoidal channels using extreme learning machines. Flow Meas. Instrum., 54: 216-223.
28. Azimi, H., H. Bonakdari and I. Ebtehaj, 2017. A highly efficient gene expression programming model for predicting the discharge coefficient in a side weir along a trapezoidal canal. Irrig. Drain., 66: 655-666.
29. French, R.H. and R.H. French, 1985. Open-Channel Hydraulics. 2nd Ed., McGraw-Hill, USA, ISBN: 9780070221345, Pages: 705.
30. Haddadi, H. and M. Rahimpour, 2012. A discharge coefficient for a trapezoidal broad-crested side weir in subcritical flow. Flow Meas. Instrum., 26: 63-67.
31. Ramamurthy, A.S., S.S. Han and P.M. Biron, 2013. Three-dimensional simulation parameters for 90° open channel bend flows. J. Comput. Civ. Eng., 27: 282-291.
32. Roache, P.J., 1994. Perspective: A method for uniform reporting of grid refinement studies. J. Fluids Eng., 116: 405-413.
33. Ferreira, C., 2001. Gene expression programming: A new adaptive algorithm for solving problems. Complex Syst., 13: 87-129.
34. Alavi, A.H. and A.H. Gandomi, 2011. A robust data mining approach for formulation of geotechnical engineering systems. Eng. Comput., 28: 242-274.
35. Shiri, J. and O. Kisi, 2011. Comparison of genetic programming with neuro-fuzzy systems for predicting short-term water table depth fluctuations. Comput. Geosci., 37: 1692-1701.
36. Ferreira, C., 2002. Gene Expression Programming in Problem Solving. In: Soft Computing and Industry-Recent Applications, Roy, R., S. Ovaska, T. Furuhashi and F. Hoffman (Eds.). Springer-Verlag, Uk, pp: 635-654.
37. Zhong, J., L. Feng and Y.S. Ong, 2017. Gene expression programming: A survey. IEEE Comput. Intell. Mag., 12: 54-72.
38. Alavi, A.H., A.H. Gandomi, H.C. Nejad, A. Mollahasani and A. Rashed, 2012. Design equations for prediction of pressuremeter soil deformation moduli utilizing expression programming systems. Neural Comput. Appl., 23: 1771-1786.
39. Azimi, H., S. Shabanlou and M.S. Salimi, 2014. Free surface and velocity field in a circular channel along the side weir in supercritical flow conditions. Flow Meas. Instrum., 38: 108-115.
40. Mohammed, A.Y. and A. Sharifi, 2020. Gene expression programming (GEP) to predict coefficient of discharge for oblique side weir. Appl. Water Sci., Vol. 10. 10.1007/s13201-020-01211-5.
41. Jain, A., K. Varshney and U. Joshi, 2001. Short-term water demand forecast modelling at IIT Kanpur using artificial neural networks. IEE Trans. Water Res. Manage., 15: 299-321.
42. Jain, A. and L.E. Ormsbee, 2002. Short-term Water demand forecast modeling techniques-Conventional methods versus AI. J. Am. Water Works Assoc., 94: 64-72.
43. Kisi, O., M.E. Karahan and Z. Sen, 2006. River suspended sediment modeling using fuzzy logic approach. Hydrol. Proc., 20: 4351-4362.